Plastic Buckling of Eccentrically Stiffened Multilayered Circular Cylindrical Shells

ROBERT M. JONES*
The Aerospace Corporation, San Bernardino, Calif.

A transcendental stability criterion is derived for plastic buckling of eccentrically stiffened circular cylindrical shells with multiple isotropic layers under combinations of axial and lateral pressure (including one component of pressure which causes tension). The deformation theory of plasticity is utilized in conjunction with classical stability theory, which implies a membrane prebuckled shape, for a set of simply supported edge boundary conditions. The uniaxial character of the stiffeners and their eccentricity (asymmetry about the reference surface) are accounted for as are variable Poisson's ratios above the yield stress (proportional limit). Coupling between bending and extension of the shell layers is included. The technique of applying this type of stability criterion is discussed for the first time and includes new procedures required for multilayered shells. Numerical examples are given to illustrate application of the theory.

Nomenclature†

a = ring spacing (Fig. 1)
A = cross-sectional area of a stiffener
A_{ij} = plasticity coefficients [Eq. (12)]
b = stringer spacing (Fig. 1)
B_{ij} = plastic buckling extensional stiffnesses of the layered shell
$\bar{B}_{ij}$ = elastic extensional stiffnesses of the layered shell
$\hat{B}_{ij}$ = plastic prebuckling extensional stiffnesses of the layered shell
c = material parameter [Eq. (25)]
C_{ij} = coupling stiffnesses of the layered shell
D_{ij} = plastic buckling bending stiffnesses of the layered shell
$\bar{D}_{ij}$ = elastic bending stiffnesses of the layered shell
$\hat{D}_{ij}$ = plastic prebuckling bending stiffnesses of the layered shell
e_i = strain intensity [(Eq. (2)]
E = Young's modulus
E_{sec} = secant modulus
E_{tan} = tangent modulus
G_{sec} = secant shearing modulus, $E_{sec}/[2(1+\nu)]$
I = moment of inertia of a stiffener about its centroid
J = torsional constant of a stiffener
$K_{ij}{}^k$ = function of material properties of the kth layer [Eq. (11)]
L = length of circular cylindrical shell (Fig. 1)
m = number of axial buckle halfwaves
M_x,M_y,M_{xy},M_{yx} = moments per unit length
n = number of circumferential buckle waves
N_x,N_y,N_{xy} = in-plane axial, circumferential, and shear forces per unit length
$\bar{N}_x,\bar{N}_y$ = applied axial and circumferential forces per unit length
R = shell reference surface radius (Figs. 1 and 2)
t_k = thickness of kth shell layer
u,v,w = axial, circumferential, and radial displacements from a membrane prebuckled shape
x,y,z = axial, circumferential, and radial coordinates on shell reference surface (Fig. 1)
$\bar{z}$ = distance from stiffener centroid to shell reference surface (Fig. 1), positive when stiffener on outside
$\epsilon_x,\epsilon_y,\gamma_{xy}$ = axial, circumferential, and shear strains
$\epsilon_1,\epsilon_2,\epsilon_3$ = variations in reference surface axial, circumferential, and shear strains [Eq. (8)]
λ = eigenvalue defined by Eq. (27)
λ_i = ith eigenvalue
ν = Poisson's ratio [Eq. (6)]
ν_e = Poisson's ratio in the elastic state
σ_i = stress intensity [Eq. (1)]
σ_{OY} = 0.2% offset yield stress
$\sigma_x,\sigma_y,\tau_{xy}$ = axial, circumferential, and shear stresses
σ_Y = yield stress (proportional limit)
χ_1,χ_2,χ_3 = variations in reference surface curvatures [Eq. (9)]

Superscript

k = kth shell layer

Subscripts

c = calculated
e = estimated
k = kth shell layer
ps = prescribed strain
r = ring
s = stringer

Received March 20, 1969; revision received August 11, 1969.

* Member of the Technical Staff, Theoretical Mechanics Section. Associate Fellow AIAA.

† A comma indicates partial differentiation with respect to the subscript following the comma. The prefix δ denotes the variation during buckling of the symbol which follows.

Introduction

THE ring- and stringer-stiffened circular cylindrical shell is a common aerospace structural element for which considerable information is available on elastic buckling, but little on plastic buckling. Gerard[1] used conventional orthotropic shell theory to represent a stiffened single-layered circular cylindrical shell, but did not account for the essentially uniaxial character of the stiffeners nor their eccentricity (asymmetry about the shell middle surface). Jones[2] corrected the aforementioned deficiencies. Peterson[3] extended Jones' work to shell configurations which have geometrical and material properties symmetrically disposed about the middle surface (including sandwich shells for which transverse shear effects are treated).

The object of the present paper is to extend previous theories to consideration of plastic buckling of eccentrically stiffened circular cylindrical shells with multiple isotropic layers which are not symmetrically disposed about a reference surface (see Figs. 1 and 2). The loading is arbitrary combinations of axial and lateral pressure including axial tension and external pressure as well as axial compression and internal pressure. Classical stability theory, which implies a membrane prebuckled shape, is used for the simply supported edge boundary conditions $\delta N_x = v = w = \delta M_x = 0$. Each layer of the thin multilayered shell is perfectly bonded to

adjacent layers; accordingly, the Kirchhoff-Love hypothesis is invoked in consonance with conventional thin shell theory.[4] Coupling between bending and extension of the layers is included in the derivation in the manner of Jones.[5] One-dimensional beam elements are used to represent the stiffeners in an approximate manner after Block, Card, and Mikulas[6] in order to account for coupling between bending and extension of the shell and stiffeners.

Simple J_2 deformation theory of plasticity (also called maximum octahedral shear stress theory, maximum energy of distortion theory, etc.) is utilized in spite of the fact that incremental theory is probably more valid for general loading histories. It is well known that incremental and deformation theories yield identical results for proportional loading equilibrium problems because in that case deformation theory is integrated incremental theory. However, Budiansky[7] shows that deformation theory is consistent with accepted incremental theory conditions even for a range of nonproportional loading around the proportional loading condition. The permissible bounds on degree of nonproportional loading are not necessarily satisfied by the deformations during buckling. However, experimental shell buckling results appear to be in reasonably good agreement with deformation theory predictions whereas the same cannot be said for incremental theory predictions. Nevertheless, more experimental evidence is required to fully substantiate the applicability of deformation theory to plastic buckling problems.

The present solution is an extension of Stowell's work[8] in which it is assumed, in accordance with Shanley's tangent modulus theory,[9] that unloading does not occur during buckling. In contrast to the constant Poisson's ratio ($\nu = \frac{1}{2}$) employed by Stowell,[8] a variable Poisson's ratio provides a smooth transition from the elastic (compressible) state to the plastic (incompressible) state with increasing stress intensity. Donnell-type stability differential equations are employed to derive a transcendental stability criterion in terms of the geometry and material properties at buckling. The technique of applying this type of stability criterion is discussed for the first time and includes new procedures required for multilayered shells. Numerical examples are given to illustrate application of the theory.

Derivation of Stability Criterion

By use of simple J_2 deformation theory of plasticity, expressions are obtained for the variation of biaxial stresses during buckling in terms of the variations of strains and material properties during buckling in each layer of a multilayered circular cylindrical shell. The variations in biaxial stresses are integrated over the shell layers and the variations in uniaxial stresses are integrated over the stiffeners in order to obtain expressions for the variations in forces and moments during buckling of a stiffened shell. Finally, the variations in forces and moments are substituted in Donnell-type stability differential equations which are solved for simply supported edge boundary conditions to yield a transcendental stability criterion in terms of the geometry and nonlinear material properties of the stiffened shell. The criterion is applicable for arbitrary combinations of axial and lateral pressure; its solution is described in a subsequent section.

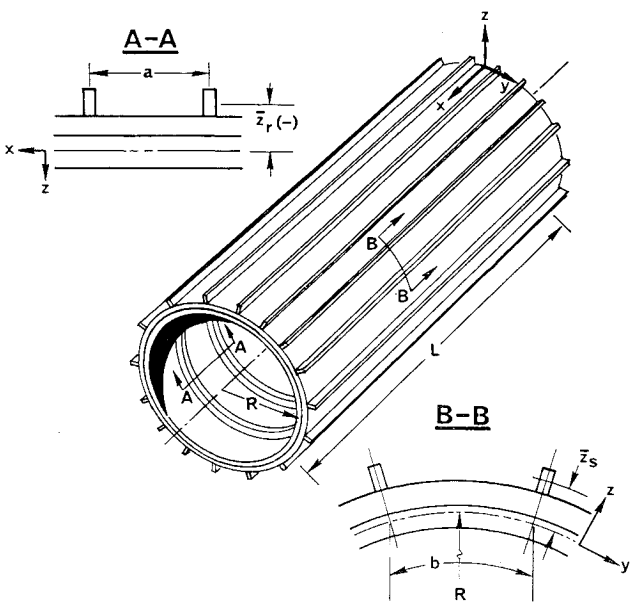

Fig. 1 Stiffened multilayered shell.

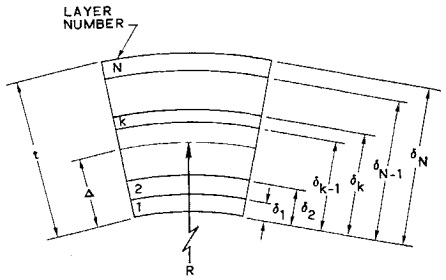

Fig. 2 Cross section of an *N*-layered shell.

Fundamental Relations in J_2 Deformation Theory

The fundamental quantities in the J_2 deformation theory of plasticity (see Nadai[10]) for the kth layer of a multilayered shell are the stress intensity, σ_{ik}

$$\sigma_{ik} = (\sigma_{xk}^2 + \sigma_{yk}^2 - \sigma_{xk}\sigma_{yk} + 3\sigma_{xyk}^2)^{1/2} \tag{1}$$

and the strain intensity, e_{ik}

$$e_{ik} = [1/(1 - \nu_k^2)][(1 - \nu_k + \nu_k^2)(\epsilon_{xk}^2 + \epsilon_{yk}^2) - (1 - 4\nu_k + \nu_k^2)\epsilon_{xk}\epsilon_{yk} + (\tfrac{3}{4})(1 - \nu_k)^2\tau_{xyk}^2]^{1/2} \tag{2}$$

The stress-strain relations which link the stress and strain intensities are

$$\left.\begin{aligned} \sigma_{xk} &= [E_{\text{sec}}^k/(1 - \nu_k^2)](\epsilon_{xk} + \nu_k\epsilon_{yk}) \\ \sigma_{yk} &= [E_{\text{sec}}^k/(1 - \nu_k^2)](\epsilon_{yk} + \nu_k\epsilon_{xk}) \\ \tau_{xyk} &= \{E_{\text{sec}}^k/[2(1 + \nu_k)]\}\gamma_{xyk} \end{aligned}\right\} \tag{3}$$

In addition, certain material properties are defined in terms of the stress and strain intensities: First, the secant modulus, E_{sec}^k

$$E_{\text{sec}}^k = \sigma_{ik}/e_{ik} \tag{4}$$

second, the tangent modulus, $E_{\tan}^k$

$$E_{\tan}^k = d\sigma_{ik}/de_{ik} \tag{5}$$

and finally a variable Poisson's ratio

$$\nu_k = \tfrac{1}{2} - (\tfrac{1}{2} - \nu_{ek})(E_{\text{sec}}^k/E^k) \tag{6}$$

where E^k is the elastic Young's modulus and ν_{ek} is the elastic Poisson's ratio. By use of Eq. (6), a smooth transition is provided between the elastic (compressible) state and the plastic (incompressible) state as the stress intensity is increased.

Variations of Strains during Buckling

In accordance with the Kirchhoff-Love hypothesis, a linear strain distribution exists during buckling. Thus, the variations of strains in the kth layer during buckling are

$$\delta\epsilon_{xk} = \epsilon_1 + z_k\chi_1, \quad \delta\epsilon_{yk} = \epsilon_2 + z_k\chi_2, \quad \delta\gamma_{xyk} = \epsilon_3 + z_k\chi_3 \tag{7}$$

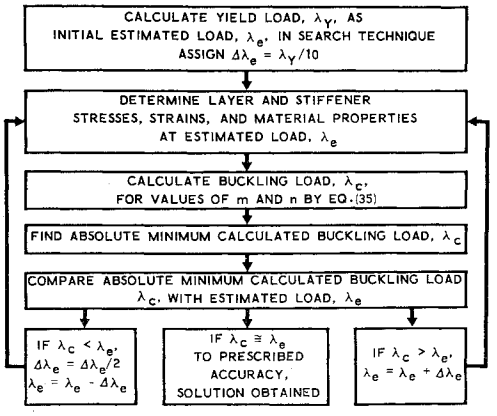

Fig. 3 Stability criterion solution procedure.

where ϵ_1, ϵ_2, and ϵ_3 are the variations of the reference surface strains

$$\epsilon_1 = u_{,x}, \qquad \epsilon_2 = v_{,y} + w/R, \qquad \epsilon_3 = u_{,y} + v_{,x} \tag{8}$$

χ_1, χ_2, and χ_3 are the variations in reference surface curvatures

$$\chi_1 = -w_{,xx} \qquad \chi_2 = -w_{,yy} \qquad \chi_3 = -2w_{,xy} \tag{9}$$

and z_k is the distance from the reference surface to the middle surface of the kth layer.

Variations of Stresses during Buckling

The variations of stresses in each layer are obtained from Eq. (3) in the manner of Jones[2] and are, for combinations of axial and circumferential stress, i.e., $\tau_{xy} = 0$,

$$\left.\begin{aligned} \delta\sigma_{xk} &= K_{11}^k(\epsilon_1 + z_k\chi_1) + K_{12}^k(\epsilon_2 + z_k\chi_2) \\ \delta\sigma_{yk} &= K_{12}^k(\epsilon_1 + z_k\chi_1) + K_{22}^k(\epsilon_2 + z_k\chi_2) \\ \delta\tau_{xyk} &= K_{33}^k(\epsilon_3 + z_k\chi_3) \end{aligned}\right\} \tag{10}$$

where

$$K_{ij}^k = [E_{\sec}^k/(1 - \nu_k^2)]A_{ij}^k \tag{11}$$

and

$$\begin{aligned} A_{11}^k &= 1 + (\kappa^k/2)[-\sigma_{xk} + \mu^k(\sigma_{yk} + \nu_k\sigma_{xk})] \times [(2 - \nu_k)\sigma_{xk} - (1 - 2\nu_k)\sigma_{yk}] \\ A_{12}^k &= \nu_k + (\kappa^k/2)[-\sigma_{xk} + \mu^k(\sigma_{yk} + \nu_k\sigma_{xk})] \times [(2 - \nu_k)\sigma_{yk} - (1 - 2\nu_k)\sigma_{xk}] \\ A_{22}^k &= 1 + (\kappa^k/2)[-\sigma_{yk} + \mu^k(\sigma_{xk} + \nu_k\sigma_{yk})] \times [(2 - \nu_k)\sigma_{yk} - (1 - 2\nu_k)\sigma_{xk}] \\ A_{33}^k &= (1 - \nu_k)/2 \end{aligned} \tag{12}$$

in which

$$\kappa^k = (1 - E_{\tan}^k/E_{\sec}^k)/(H^k\sigma_{ik}^2) \tag{13}$$

and

$$\mu^k = (1 - 2\nu_k)/[2(1 - \nu_k^2)] \tag{14}$$

where H^k is defined in Ref. 2.

The variations of the stiffener stresses during buckling from a membrane prebuckled shape are obtained by varying the normal stresses

$$\sigma_{xs} = E_{\sec_s}\epsilon_{xs}, \qquad \sigma_{yr} = E_{\sec_r}\epsilon_{yr} \tag{15}$$

and from the last of Eq. (10) as

$$\begin{aligned} \delta\sigma_{xs} &= E_{\tan_s}\delta\epsilon_{xs}, & \delta\sigma_{yr} &= E_{\tan_r}\delta\epsilon_{yr} \\ \delta\tau_{xys} &= G_{\sec_s}\delta\gamma_{xys}, & \delta\tau_{xyr} &= G_{\sec_r}\delta\gamma_{xyr} \end{aligned} \tag{16}$$

Note that the variations of shear stress are not obtained from uniaxial relations in parallel to Eq. (15) because such relations do not apply when no shear strain exists prior to buckling.

Variations of Forces and Moments during Buckling

The variations of forces and moments during buckling are obtained by integration of the variations of stresses over the shell layers and stiffeners. The effect of the stiffeners is averaged or "smeared out" over the stiffener spacing, e.g.,

$$\delta N_x = \sum_{k=1}^{N} \int_{t_k} \delta\sigma_{xk}dz + \frac{1}{b}\int_{A_s} \delta\sigma_{xs}dA_s \tag{17}$$

where t_k denotes the thickness of the kth layer and N is the number of layers. Integration yields

$$\left.\begin{aligned} \delta N_x &= (B_{11} + E_{\tan_s}A_s/b)\epsilon_1 + B_{12}\epsilon_2 + (C_{11} + \bar{z}_sE_{\tan_s}A_s/b)\chi_1 + C_{12}\chi_2 \\ \delta N_y &= B_{12}\epsilon_1 + (B_{22} + E_{\tan_r}A_r/a)\epsilon_2 + C_{12}\chi_1 + (C_{22} + \bar{z}_rE_{\tan_r}A_r/a)\chi_2 \\ \delta N_{xy} &= B_{33}\epsilon_3 + C_{33}\chi_3 \end{aligned}\right\} \tag{18}$$

$$\left.\begin{aligned} \delta M_x &= (C_{11} + \bar{z}_sE_{\tan_s}A_s/b)\epsilon_1 + C_{12}\epsilon_2 + (D_{11} + \bar{z}_s^2E_{\tan_s}A_s/b + E_{\tan_s}I_s/b)\chi_1 + D_{12}\chi_2 \\ \delta M_y &= C_{12}\epsilon_1 + (C_{22} + \bar{z}_rE_{\tan_r}A_r/a)\epsilon_2 + D_{12}\chi_1 + (D_{22} + \bar{z}_r^2E_{\tan_r}A_r/a + E_{\tan_r}I_r/a)\chi_2 \\ \delta M_{xy} &= -C_{33}\epsilon_3 - (D_{33} + G_{\sec_s}J_s/2b)\chi_3 \\ \delta M_{yx} &= C_{33}\epsilon_3 + (D_{33} + G_{\sec_r}J_r/2a)\chi_3 \end{aligned}\right\} \tag{19}$$

where

$$\left.\begin{aligned} B_{ij} &= \sum_{k=1}^{N} K_{ij}^k(\delta_k - \delta_{k-1}) \\ C_{ij} &= \frac{1}{2}\sum_{k=1}^{N} K_{ij}^k[(\delta_k^2 - \delta_{k-1}^2) - 2\Delta(\delta_k - \delta_{k-1})] \\ D_{ij} &= \frac{1}{3}\sum_{k=1}^{N} K_{ij}^k[(\delta_k^3 - \delta_{k-1}^3) - 3\Delta(\delta_k^2 - \delta_{k-1}^2) + 3\Delta^2(\delta_k - \delta_{k-1})] \end{aligned}\right\} \tag{20}$$

in which N is the number of layers, δ_k is the distance from the inner surface of the layered shell to the outer surface of the kth layer, and Δ is the distance from the inner surface of the layered shell to the reference surface. The stiffnesses in Eq. (20) are due to Ambartsumyan[4] and depend on the location of the reference surface (see Fig. 2). In Eq. (20), B_{ij} and D_{ij} are plastic buckling extensional and bending stiffnesses, respectively, whereas the C_{ij} are coupling stiffnesses. The elastic extensional and bending stiffnesses, $\bar{B}_{ij}$ and $\bar{D}_{ij}$, are obtained by using elastic values of $A_{ij}^k[A_{11}^k = A_{22}^k = 1$, $A_{12}^k = \nu_k$, and $A_{33}^k = (1 - \nu_k)/2]$, elastic moduli and elastic Poisson's ratios in Eqs. (15) and (20). The plastic prebuckling extensional and bending stiffnesses, $\hat{B}_{ij}$ and $\hat{D}_{ij}$, are obtained by using the elastic values of A_{ij}^k, plastic secant moduli, and plastic Poisson's ratios in Eqs. (15) and (20).

Stability Criterion

The following buckling displacements:

$$\left.\begin{aligned} u &= \bar{u}\cos(m\pi x/L)\cos(ny/R) \\ v &= \bar{v}\sin(m\pi x/L)\sin(ny/R) \\ w &= \bar{w}\sin(m\pi x/L)\cos(ny/R) \end{aligned}\right\} \tag{21}$$

satisfy the simply supported edge boundary conditions $\delta N_x = v = w = \delta M_x = 0$ and are substituted [along with the variations of forces and moments during buckling, Eqs. (18) and (19), and the variations of reference surface strains and changes of curvature, Eqs. (8) and (9)] in the Donnell-type stability differential equations for circular cylindrical shells subjected to combinations of axial and lateral pressure

$$\left.\begin{aligned} \delta N_{x,x} + \delta N_{xy,y} &= 0 \\ \delta N_{xy,x} + \delta N_{y,y} &= 0 \\ -\delta M_{x,xx} + \delta M_{xy,xy} - \delta M_{yx,xy} - \delta M_{y,yy} + \delta N_y/R + & \\ \bar{N}_x w_{,xx} + \bar{N}_y w_{,yy} &= 0 \end{aligned}\right\} \quad (22)$$

In order to obtain a nontrivial solution to the resulting homogeneous equations in $\bar{u}$, $\bar{v}$, and $\bar{w}$, i.e., an exact solution to the stability differential equations, the determinant of the coefficients of $\bar{u}$, $\bar{v}$, and $\bar{w}$ must be zero, and the following stability criterion results:

$$\bar{N}_x(m\pi/L)^2 + \bar{N}_y(n/R)^2 = a_{33} + a_{23}\left(\frac{a_{13}a_{12} - a_{11}a_{23}}{a_{11}a_{22} - a_{12}^2}\right) + a_{13}\left(\frac{a_{12}a_{23} - a_{13}a_{22}}{a_{11}a_{22} - a_{12}^2}\right) \quad (23)$$

where

$$\left.\begin{aligned} a_{11} &= (B_{11} + E_{\tan_s}A_s/b)(m\pi/L)^2 + B_{33}(n/R)^2 \\ a_{12} &= (B_{12} + B_{33})(m\pi/L)(n/R) \\ a_{13} &= (B_{12}/R)(m\pi/L) + (C_{11} + \bar{z}_s E_{\tan_s}A_s/b) \times \\ &\quad (m\pi/L)^3 + (C_{12} + 2C_{33})(m\pi/L)(n/R)^2 \\ a_{22} &= B_{33}(m\pi/L)^2 + (B_{22} + E_{\tan_r}A_r/a)(n/R)^2 \\ a_{23} &= (C_{12} + 2C_{33})(m\pi/L)^2(n/R) + \\ &\quad (1/R)\,(B_{22} + E_{\tan_r}A_r/a)(n/R) + \\ &\quad (C_{22} + \bar{z}_r E_{\tan_r}A_r/a)(n/R)^3 \\ a_{33} &= (D_{11} + E_{\tan_s}I_s/b + \bar{z}_s^2 E_{\tan_s}A_s/b)(m\pi/L)^4 + \\ &\quad (4D_{33} + 2D_{12} + G_{\sec_s}J_s/b + G_{\sec_r}J_r/a) \times \\ &\quad (m\pi/L)^2(n/R)^2 + (D_{22} + E_{\tan_r}I_r/a + \bar{z}_r^2 E_{\tan_r}A_r/a) \times \\ &\quad (n/R)^4 + (2C_{12}/R)(m\pi/L)^2 + (2/R)(C_{22} + \\ &\quad \bar{z}_r E_{\tan_r}A_r/a)(n/R)^2 + (1/R^2)(B_{22} + E_{\tan_r}A_r/a) \end{aligned}\right\} \quad (24)$$

Equation (23) is a transcendental expression for the buckling forces $\bar{N}_x$ and $\bar{N}_y$ in terms of the material properties at $\bar{N}_x$ and $\bar{N}_y$ and in terms of the geometry and buckling mode numbers. The stability criterion represented by Eq. (23) reduces to Jones' solution[2] for plastic buckling of stiffened single-layered shells; Jones' solution[5] for elastic buckling of stiffened multilayered shells; Block, Card, and Mikulas' solution[6] for stiffened elastic single-layered shells; and the classical Euler solution for unstiffened elastic shells. The solution of Eq. (23) for the lowest buckling load is discussed in the next section.

Solution of Stability Criterion

The buckling load calculated from Eq. (23) depends on the geometry, buckling mode parameters, m and n, and material properties. However, the material properties are a function of the buckling load. Thus, Eq. (23) is a transcendental expression and because of this and the numerous geometric and material properties, a computer program[11] is essential to the practical calculation of buckling loads. Actually, the major portion of the effort in analysis of plastic buckling of shells is in the solution of the transcendental stability criterion. However, little, if any, discussion of the solution procedure is published. Description of the solution procedure is especially important for multilayered shells because of required new techniques.

The solution procedure is displayed schematically in Fig. 3 and is outlined in the following sentences; each step is described in the following subsections. The objective of the solution procedure is to logically estimate a succession of loads to search for the load at which the stiffened multilayered shell buckles according to the transcendental stability criterion, Eq. (23). The first step is to calculate the yield load, λ_Y, to determine the boundary between elastic and plastic behavior (λ_Y is the basis for a decision in a later step). The second step is to determine the layer and stiffener stresses, strains, and, hence, material properties at an estimated load by a succession of numerical techniques (with the exception that at the first estimated load, λ_Y, the material properties are elastic so the stresses and strains can be determined directly). The third step is to calculate the buckling load for each value of m and n at the material properties corresponding to the estimated load and to select the absolute minimum calculated buckling load from among values for a prescribed range of m and n. The fourth and final step is to compare the absolute minimum calculated buckling load with the estimated buckling load to determine whether the solution has been obtained. For the first estimated buckling load, λ_Y, if the absolute minimum calculated buckling load is less than the yield load, buckling is elastic and the solution has been obtained. If it is greater than the yield load, a searching technique is developed herein for choosing a succession of estimated loads and repeating steps two through four until the estimated plastic buckling load is the same as the absolute minimum calculated plastic buckling load to a prescribed accuracy. The searching technique is displayed in Fig. 3 and described in a subsequent section.

The stiffened multilayered shell is represented by its geometry and by nonlinear stress-strain curves for each layer and stiffener. The Nadai stress-strain curve for a 0.2% offset yield stress is used for the purposes of illustration

$$\begin{aligned} &\sigma_i \le \sigma_Y; \quad e_i = \sigma_i/E \\ &\sigma_i > \sigma_Y; \quad e_i = \sigma_i/E + 0.002[(\sigma_i - \sigma_Y)/(\sigma_{OY} - \sigma_Y)]^c \end{aligned} \quad (25)$$

although any other nonlinear stress-strain relations can be used if desired. The stiffeners and each layer can have different values of E, ν, σ_Y, σ_{OY}, and c in the author's computer program.[11]

Determination of the Yield Load

In the axisymmetric elastic membrane prebuckled state, the force-strain relations are given by

$$\begin{aligned} \bar{N}_x &= (\bar{B}_{11} + E_sA_s/b)\bar{\epsilon}_x + \bar{B}_{12}\bar{\epsilon}_y \\ \bar{N}_y &= \bar{B}_{12}\bar{\epsilon}_x + (\bar{B}_{22} + E_rA_r/a)\bar{\epsilon}_y \end{aligned} \quad (26)$$

Let N_x and N_y be related to a positive number λ which represents the loading in the following manner

$$\bar{N}_x = k_1\lambda, \qquad \bar{N}_y = k_2\lambda \quad (27)$$

where k_1 and/or k_2 can be negative, although it is to be noted that buckling occurs only when either k_1 or k_2 is positive. The objective of this section is to find the value of λ which will cause yielding in one layer of the shell or in the stiffeners. To this end, let

$$\begin{aligned} AA &= \bar{B}_{11} + E_sA_s/b, \qquad BB = \bar{B}_{12} \\ CC &= \bar{B}_{22} + E_rA_r/a \end{aligned} \quad (28)$$

Equations (26–28) can be written as

$$k_1\lambda = AA\bar{\epsilon}_x + BB\bar{\epsilon}_y, \qquad k_2\lambda = BB\bar{\epsilon}_x + CC\bar{\epsilon}_y \quad (29)$$

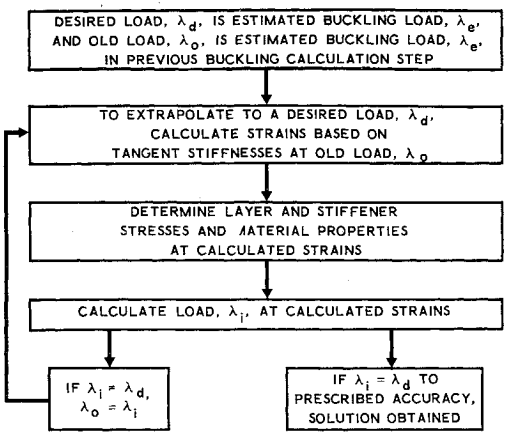

Fig. 4 Procedure for determination of layer and stiffener stresses, strains, and material properties at the estimated buckling load.

Upon solution of Eq. (29) for $\bar{\epsilon}_x$

$$\bar{\epsilon}_x = [(BBk_2 - CCk_1)/(BB^2 - AACC)]\lambda = \bar{A}\lambda \quad (30)$$

Similarly,

$$\bar{\epsilon}_y = [(k_1 - AA\bar{A})/BB]\lambda = \bar{B}\lambda \quad (31)$$

so the membrane strains are known in terms of the applied loads. Upon substitution of the membrane strains in the expression for the strain intensity in the kth layer

$$e_{ik} = [1/(1 - \nu_k^2)][(1 - \nu_k + \nu_k^2)(\bar{A}^2 + \bar{B}^2) - (1 - 4\nu_k + \nu_k^2)\bar{A}\bar{B}]^{1/2}\lambda \quad (32)$$

and conversion to the stress intensity in the kth layer by use of Eq. (4), the load causing yielding in the layered shell is the smallest of

$$\lambda_{Yk} = \sigma_{Yk}/E^k\bar{C}_k \quad (33)$$

where $\bar{C}_k$ is the coefficient of λ in Eq. (32). For the rings, the load which causes yielding is

$$\lambda_{Yr} = |\sigma_{Yr}/E_r\bar{B}| \quad (34)$$

whereas for the stringers, the load which causes yielding is

$$\lambda_{Ys} = |\sigma_{Ys}/E_s\bar{A}| \quad (35)$$

The yield load for the stiffened shell is the smallest of the λ in Eqs. (33–35). The yield load, of course, separates the elastic behavior of the shell from the nonlinear behavior. The stresses and strains at the yield load are obtained by substitution of the smallest λ in Eqs. (30, 31, and 3) successively.

Determination of Layer and Stiffener Stresses, Strains, and Material Properties at an Estimated Buckling Load

In order to determine the layer and stiffener stresses, strains, and material properties at an estimated buckling load, the load-deformation behavior of the stiffened multilayered shell must first be determined. For single-layered shells in a membrane prebuckling equilibrium state, the load-deformation behavior is merely a scaling constant times the stress-strain behavior. However, multilayered shells, even in a membrane prebuckling equilibrium state, exhibit much more complex behavior because no such scaling constant exists. Although the axial, as well as the circumferential, strain is the same in each layer, the strain intensity, Eq. (2), is not the same because the Poisson's ratio is different in each layer.

Actually, at this stage in the solution, only a portion of the load-deformation behavior is required, namely, the determination of the deformation at the estimated buckling load. At each such required determination in the search for the buckling load, the necessary steps are shown in Fig. 4 and described as follows. The associated numerical techniques are explained in more detail in the following paragraphs. First, the load-deformation curve is extrapolated from a known point to the new estimated load, λ_d, at which the strains are calculated using the material properties of the known point. The second step is to calculate the layer and stiffener stresses and material properties at the strains calculated in the first step. The third step is to calculate the actual load from the layer and stiffener stresses at the calculated strains and compare it to the desired load. If the calculated load is not equal to the desired load, a new (smaller) load increment is determined by the difference between the calculated and desired loads. The steps are repeated until the calculated load is the same as the desired load to a prescribed accuracy. Three broad classes of iterations are noted in Figs. 3 and 4: 1) load estimates; 2) strain estimates; and 3) layer and stiffener stress estimates. The number of iterations, subiterations, and subsubiterations that must be undergone is highly dependent on the degree of nonlinearity of the stress-strain curves and on the geometry of the configuration. The number of iterations, etc., for a particular case are given in the Numerical Example Section.

The extrapolation procedure, or tangent predictor technique, can best be explained by reference to Fig. 5 in the following discussion. In Fig. 5, λ is the load and Δ is a characteristic deformation. The tangent extensional stiffnesses, B_{ij}, are used to extrapolate from the old load, λ_o, at the previous known deformation (starting with the yield deformation and load at the beginning of the entire procedure to solve the stability criterion) to the desired load, λ_d, at which the deformation is to be determined. If an increment in λ is formed in the manner of Eq. (27), the prebuckling force-strain relations

$$\left.\begin{aligned}\bar{N}_x &= (\hat{B}_{11} + E_{\sec_s}A_s/b)\bar{\epsilon}_x + \hat{B}_{12}\bar{\epsilon}_y\\ \bar{N}_y &= \hat{B}_{12}\bar{\epsilon}_x + (\hat{B}_{22} + E_{\sec_r}A_r/a)\bar{\epsilon}_y\end{aligned}\right\} \quad (36)$$

can be written in incremental form

$$\left.\begin{aligned}\Delta\bar{N}_x &= (B_{11} + E_{\tan_s}A_s/b)\Delta\bar{\epsilon}_x + B_{12}\Delta\bar{\epsilon}_y\\ \Delta\bar{N}_y &= B_{12}\Delta\bar{\epsilon}_x + (B_{22} + E_{\tan_r}A_r/a)\Delta\bar{\epsilon}_y\end{aligned}\right\} \quad (37)$$

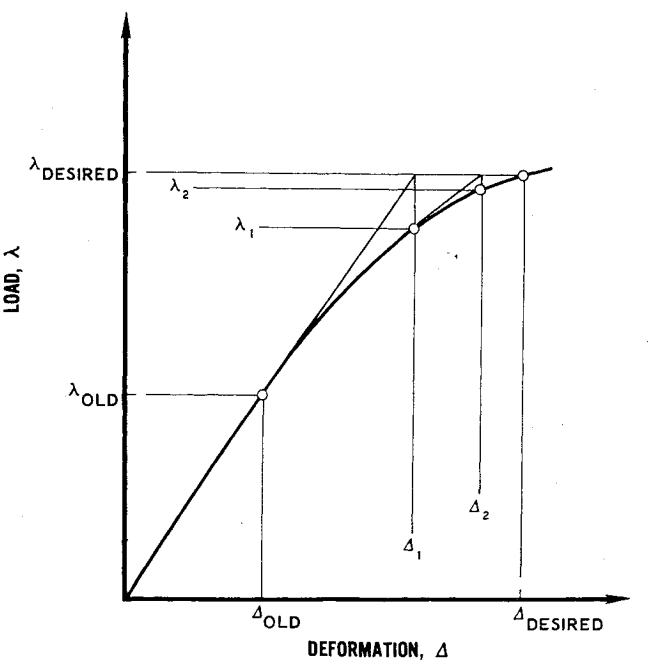

Fig. 5 Tangent predicator technique for obtaining load-deformation curve.

The increments in strain determined from Eq. (37) when added to the old strains constitute an approximation to the strains (or deformation, Δ_1) at the desired λ_d. The question remains to determine the actual λ_1 which corresponds to Δ_1. A procedure is described in the next two paragraphs for determining the layer and stiffener stresses and material properties at the strains calculated from Eq. (37) corresponding to Δ_1. After the actual λ_1 is determined, another trial value, Δ_2, of the strains at the desired λ_d is obtained and the procedure is repeated until λ_i agrees with λ_d to a prescribed accuracy. In Fig. 5, only two approximations are shown as further approximations are so close to the desired solution as to be indistinguishable at the scale of Fig. 5.

A set of strains for the layered shell is determined in the preceding paragraph. Because of the membrane prebuckled equilibrium state, the strains are equal in all layers so the strains in each layer are known a priori. However, the material properties, and hence the stresses, are not known in each layer. The stresses are determined for each layer by forming e_{ipsk},

$$e_{ipsk} = [1/(1 - \nu_k^2)][(1 - \nu_k + \nu_k^2)(\bar{\epsilon}_x^2 + \bar{\epsilon}_y^2) - (1 - 4\nu_k + \nu_k^2)\bar{\epsilon}_x\bar{\epsilon}_y]^{1/2} \quad (38)$$

the strain intensity determined by the prescribed strains and material properties at a given stress intensity, and searching by an interval halving technique for the stress intensity with a corresponding strain intensity, e_{ik}, which agrees with e_{ipsk} to a prescribed degree of accuracy. A schematic indication of the aforementioned procedure is given for a single layer in Fig. 6. There, it is noted that $e_{ips1} > e_{i1}$ so the stress intensity is increased by $\Delta\sigma_i$ to σ_{i2}. At σ_{i2}, $e_{ips2} < e_{i2}$ so σ_i is decreased by $\Delta\sigma_i/2$ to σ_{i3} where $e_{ips3} > e_{i3}$. Then, σ_i is increased by $\Delta\sigma_i/4$ to σ_{i4} at which point $e_{ips4} < e_{i4}$. The interval halving is repeated to continually bound the correct solution closer from above and below until $e_{ips} = e_i$ to the desired accuracy. The last step is to calculate the stresses from Eq. (3) when the material properties are obtained from the Nadai stress-strain curve for the determined stress intensity.

The stress in the stiffeners is found by use of the tangent predictor technique for determining uniaxial stress at a prescribed uniaxial strain as illustrated schematically in Fig. 7.

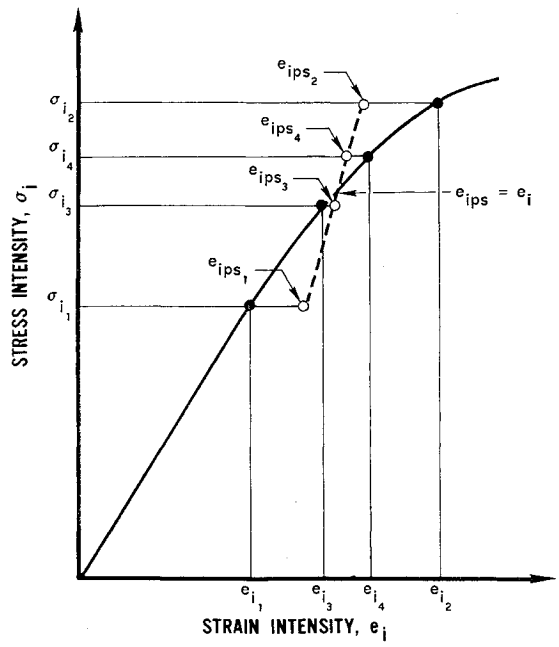

Fig. 6 Determination of stress intensity and strain intensity for given $\bar{\epsilon}_x$ and $\bar{\epsilon}_y$.

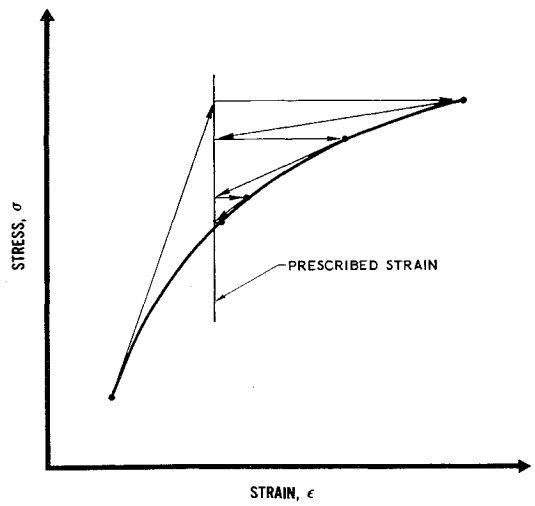

Fig. 7 Tangent predicator technique for determining uniaxial stress at a prescribed uniaxial strain.

The ring stress, for example, is given an increment

$$\Delta\sigma_y = E_{\tan_r}\Delta\epsilon_{yr} \quad (39)$$

where $\Delta\epsilon_{yr}$ is initially the difference between the prescribed strain and some convenient initial value of strain, say the value at the previous load (at which $E_{\tan_r}$ is also evaluated). The new strain, ϵ_{yr}, corresponding to the new stress is calculated by use of the Nadai stress-strain relation for the stiffener. Since the new strain does not agree with the prescribed strain, their difference is used in Eq. (39) to obtain a new stress and strain. The procedure is repeated until the new strain agrees with the prescribed strain to the desired accuracy thereby determining the stress and material properties of the stiffener at the prescribed strain. This relatively simple procedure is unsuitable for the determination of stresses in a layered shell since the prescribed strains do not determine a unique strain intensity from which to calculate incremental strain. Accordingly, in that case the search for a solution would be somewhat like a cat chasing its tail.

Calculation of the Absolute Minimum Buckling Load at an Estimated Load

The buckling load calculated by use of Eq. (23) is actually a function of the buckling mode parameters, m and n, as well as the material properties at the estimated load. The following discussion pertains to the determination of the absolute minimum of the values of the calculated buckling load, λ_c, for a wide range of m and n.

First, the relative minima of λ_c for a series of fixed values of m are found by varying n over a prescribed range as in Fig. 8a. The absolute minima of the λ_c for each value of m are then compared to find the absolute minimum λ_c for all m and n in Fig. 8b. The aforementioned procedure of searching for an absolute minimum λ_c for discrete values of m and n is necessary because of the possibility, for stiffened shells, of obtaining more than one relative minimum as in Fig. 8b. In such cases, ordinary procedures of determining a stationary value of λ_c by differentiating λ_c with respect to m and n and equating the results to zero are totally inadequate and misleading. The sign of the second derivative must be examined in order to determine whether a minimum, maximum, or inflection point has been obtained by the stationary value procedure which many individuals erroneously call "minimization." Actually, the determination of such derivatives and the associated logic for selection of the absolute minimum would result in undesirable noninteger values of m and n and would take about the same effort as the procedure used herein. The present search procedure obviates the need

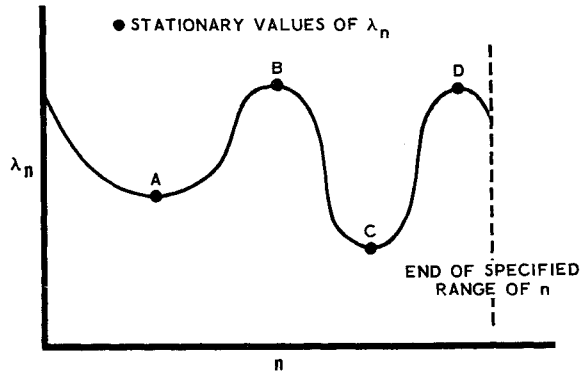

a) Values of λ for each value of n when m is fixed.

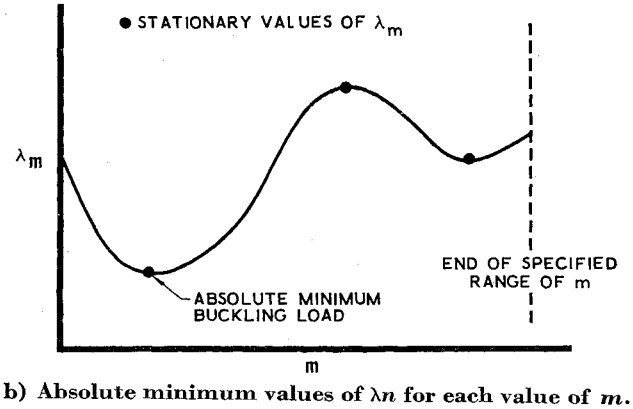

b) Absolute minimum values of λn for each value of m.

Fig. 8 Determination of absolute minimum buckling load.

for determining any derivatives of λ_c, but is subject to the limitation that a sufficiently wide range of m and n must be prescribed or the absolute minimum can be missed, i.e., the range of m and n must include the values for the true absolute minimum. Two factors ease the difficulty in deciding on the range of m and n to be investigated: 1) practical experience and 2) the computer program developed by the author[11] notes behavior such as a decreasing λ_c as the end of the range of n (or m) is approached, e.g., Fig. 8a, and prints a message that the range of n (or m) should be increased. These two factors lead to reasonable assurance that no relative minimum which might be the absolute minimum is missed.

Comparison of Estimated and Absolute Minimum Calculated Buckling Load

The buckling load which is calculated from Eq. (23) must coincide with the estimated load for which the material properties in Eq. (23) apply in order for the plastic buckling solution to have been found. If the estimated load, λ_e, is too low, the calculated load, λ_c, is too high because the material properties are too high. Conversely, if λ_e is too high, λ_c is too low. Thus, the aforementioned relation of λ_e to λ_c is an ideal criterion for use in a numerical technique to determine where λ_c equals λ_e to a prescribed accuracy.

Various load estimates, λ_{ie}, are made in Fig. 9 on the load-deformation curve and corresponding absolute minimum calculated buckling loads are obtained by procedures discussed previously. The first load estimate, λ_{ie}, is the previously determined yield load for which the corresponding λ_{ic} is too high in Fig. 9 because the material properties are too high. Successive load increments, $\Delta\lambda$, of one-tenth the yield load are added until λ_{ic} is less than λ_{ie}, e.g., $\lambda_{4c} < \lambda_{4e}$ in Fig. 9. At this point, the estimated load is reduced by $\Delta\lambda/2$. The new λ_{ie} is compared to the corresponding λ_{ic} whereupon λ_{ie} is increased by $\Delta\lambda/4$ or decreased by $\Delta\lambda/2$ according to whether $\lambda_{ic} > \lambda_{ie}$ or $\lambda_{ic} < \lambda_{ie}$ as in Fig. 3. The load increment is halved at essentially each step until $\lambda_{ic} = \lambda_{ie}$ to a prescribed accuracy. This interval halving search procedure converges by virtue of the relation of λ_e to λ_c and can be shown to be the most efficient search procedure. The iteration procedures which were attempted for the determination of where λ_e equals λ_c did not converge.

Numerical Examples

As mentioned in the Introduction, the numerous geometrical and material parameters in the present investigation cannot be nondimensionalized in a meaningful fashion, i.e., general results cannot be presented. Accordingly, two numerical examples are given in order to illustrate application of the present theory. The first example is illustrative of the new capability represented by the present theory in that a heretofore unattacked problem, plastic buckling of a ring-stiffened, four-layered shell under hydrostatic pressure, is solved. The second example is a re-examination of a ring- and stringer-stiffened shell which is representative of current large diameter booster interstage structures. The buckling of the latter shell under axial compression was studied by Jones[2] and is examined in order to illustrate the capability of the present theory to treat negative loading components, e.g., internal pressurization of axially compressed shells or axial tension on a shell subjected to lateral pressure.

Ring-Stiffened Four-Layered Shell under Hydrostatic Pressure

A ring-stiffened four-layered shell is examined as, for example, a simulation of configurations with in-plane material properties which vary in the radial direction due to thermal degradation. Contrived material properties given in Table 1 are used in order to simplify the illustration. The corresponding stress-strain curves are shown in Fig. 10. The rings are of the same material as the first layer and are 0.25 in. high, 0.06 in. thick, and have a spacing which is varied in the present example. The basic shell is 12 in. long, has a radius of 6 in. to the reference surface which is chosen to be the center of the innermost layer, and has four layers of unequal thickness ($t_1 = 0.040$ in., $t_2 = 0.030$ in., $t_3 = 0.020$ in., and $t_4 = 0.010$ in.).

General instability (i.e., buckling in which the rings participate) results for a varying ring spacing are shown in Fig. 11 in which plastic buckling is denoted by the solid curve and elastic buckling is denoted by the dashed curve. Panel instability (i.e., buckling between rings) results are shown in Fig. 12 with the same notation as in Fig. 11. In both Figs.

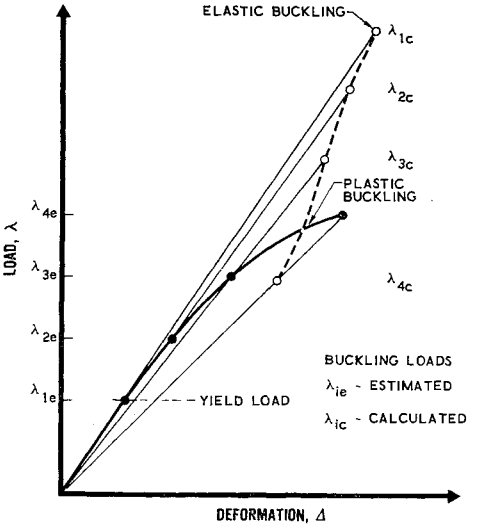

Fig. 9 Comparison of estimated and calculated buckling loads.

Table 1 Material properties of a four-layered configuration

Layer	E, psi	ν_e	c	σ_Y, psi	σ_{OY}, psi
1	10×10^6	0.20	2.0	20×10^3	30×10^3
2	6×10^6	0.25	3.0	9×10^3	13.5×10^3
3	4×10^6	0.30	4.0	4×10^3	6×10^3
4	2×10^6	0.35	5.0	1×10^3	1.5×10^3

11 and 12, cusps are noted at ring spacings where a layer (or ring) yields and where the buckling mode shape changes. A typical load-deformation curve is shown in Fig. 13 (for $a = 1.5$ in.) wherein elastic behavior is denoted by a dashed line and plastic behavior is denoted by a solid curve. The results for Fig. 13 require about 1.4 sec of CDC 6600 central processor time (an IBM 360/65 FORTRAN G system takes about three times as long). During that time, there are 38 load estimates, 2–3 strain estimates per load estimate, 15–25 layer stress intensity estimates per strain estimate, and 1–3 stiffener stress estimates per strain estimate.

If a balance between general and panel instability were sought for the elastic case in Figs. 11 and 12, the "optimum" ring spacing is 7 in. at a buckling pressure of 180 psi. However, when plastic effects are accounted for, the "optimum" ring spacing is 5 in. at a buckling pressure of 175 psi. Perhaps more important is the fact that at a ring spacing of 7 in., the elastic buckling pressure is 26% higher than the plastic buckling pressure.

From an analysis, rather than a design, viewpoint, the neglect of plastic effects in the present example results in the buckling pressure being overestimated by from 20% to 90% as the ring spacing varies over the practical range from 4 in.–0.5 in. In addition, it can be noted by comparison of Figs. 11 and 12 that the general and panel instability results are much closer to each other for the plastic case than for the elastic case.

A configuration like the aforementioned example except with four layers, each 0.020-in. thick, yields slightly different results. The optimum ring spacing changes from 3.5 in. in the elastic case to about 1 in. in the plastic case. A striking observation is the fact that, due to plastic effects, panel instability governs over nearly the entire range of stiffener spacings in contrast to the elastic case for which general instability governs over a wide range of stiffener spacings. In addition, the rings of the equal thickness four-layered shell yield at a ring spacing noticeably different from the ring spacing at which the innermost layer (to which the rings are fastened) yields.

Stiffened Large Diameter Booster Interstage Structure under Biaxial Loading

A ring- and stringer-stiffened aluminum shell which is representative of large diameter booster interstage structures

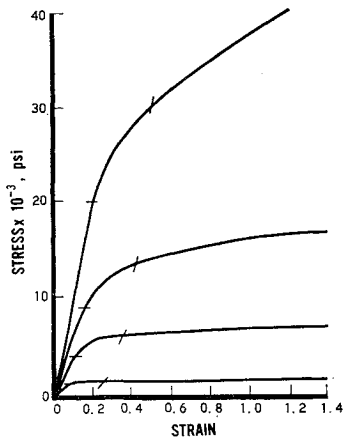

Fig. 10 Stress-strain curves for four contrived materials.

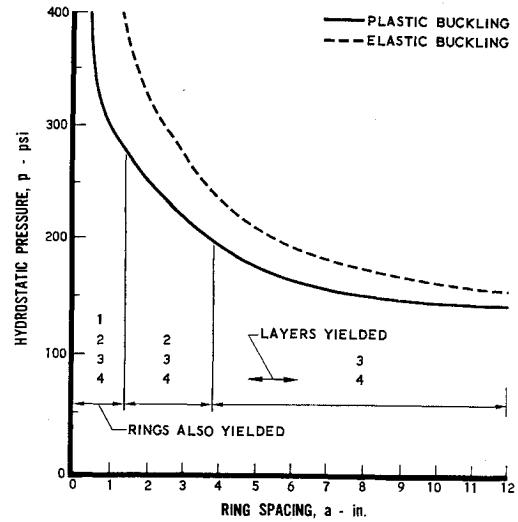

Fig. 11 General instability of a ring-stiffened four-layered circular cylindrical shell under hydrostatic pressure.

is subjected to biaxial loading, including axial tension and internal pressure. The geometry and material properties are given by Jones[2] in his study of the behavior of this configuration under axial compression.

General instability results under biaxial loading are displayed in Fig. 14. The yield curve, which is denoted by a dashed line with intermittent dots, separates the regions of elastic and plastic behavior. Substantial reductions, especially at large axial tension or large internal pressure, from the elastic results (dashed curve) are noted for the plastic results (solid curve).

For boosters, it is sometimes desired to increase the resistance to buckling under axial compression by use of internal pressurization, e.g., the Atlas missile. In the present example, the net axial buckling force decreases with internal pressurization due to effects of plastic deformation on the buckling resistance. When this result is compared with the prediction of increasing net axial buckling force with internal pressurization under elastic conditions, it is obvious that substantial modification must be made to the usual conclusion that internal pressurization increases the buckling resistance of boosters. Although some benefit is obtained by use of internal pressurization, the elastic approach would result in an overestimate of the axial buckling load by 30% at 100-psi internal pressure. Similar results are obtained for the use of

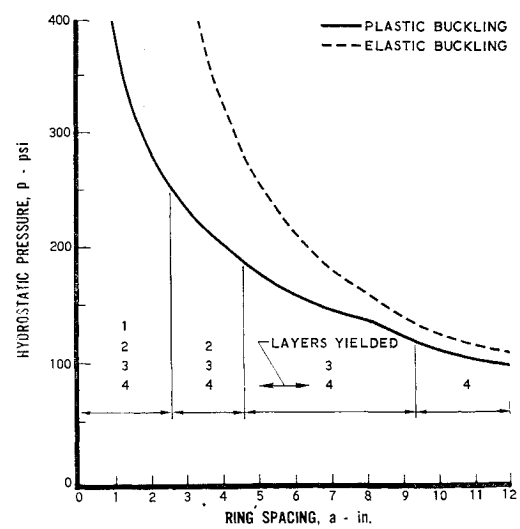

Fig. 12 Panel instability of a ring-stiffened four-layered circular cylindrical shell under hydrostatic pressure.

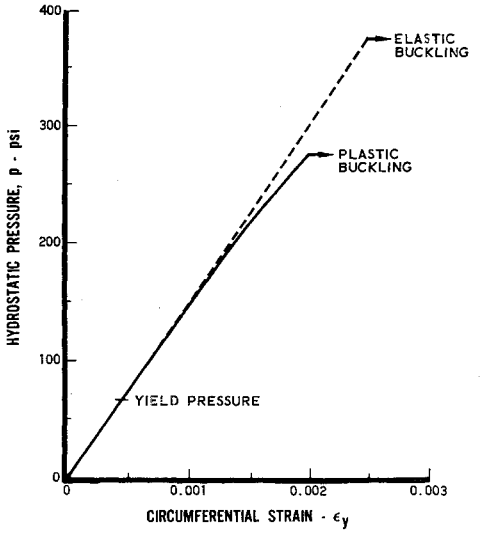

Fig. 13 Load-deformation curve for a ring-stiffened four-layered circular cylindrical shell under hydrostatic pressure.

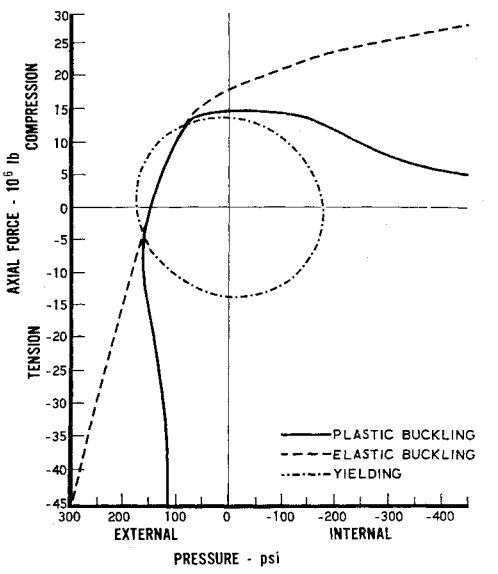

Fig. 14 Buckling of a large diameter booster interstage structure with internal rings and external stringers under biaxial loading.

axial tension to increase the buckling resistance under lateral pressure.

Concluding Remarks

A transcendental stability criterion is derived for plastic buckling of eccentrically stiffened circular cylindrical shells with multiple isotropic layers under combinations of axial and lateral pressure (including one component of pressure which causes tension). The deformation theory of plasticity is utilized in conjunction with classical stability theory, which implies a membrane prebuckled shape, for a set of simply supported edge boundary conditions. The technique of applying this type of stability criterion is discussed for the first time and includes new procedures required for multilayered shells.

The numerous geometrical and material parameters in the present investigation cannot be nondimensionalized in a meaningful fashion, i.e., general results cannot be presented. Accordingly, two numerical examples are given to illustrate application of the derived theory. The first example is a ring-stiffened four-layered shell under hydrostatic pressure. For one case, plastic effects result in a decrease of the optimum ring spacing from the value predicted by use of an elastic solution. In addition, it is shown that over a practical range of ring spacing, elastic results are from 20–90% too high. In another case, plastic effects result in panel instability governing over a much wider range of ring spacings than under elastic conditions. The second numerical example involves a ring- and stringer-stiffened aluminum shell which is representative of a large diameter booster interstage structure subjected to biaxial loading (including axial tension or internal pressure). Because of plastic effects, the benefit of internally pressurizing an axially compressed shell is substantially reduced. Similar results occur when axial tension is used to stabilize an externally pressurized shell.

References

[1] Gerard, G., "Plastic Stability Theory of Geometrically Orthotropic Plates and Cylindrical Shells," *Journal of the Aerospace Sciences*, Vol. 29, No. 8, Aug. 1962, pp. 956–962.

[2] Jones, R. M., "Plastic Buckling of Eccentrically Stiffened Circular Cylindrical Shells," *AIAA Journal*, Vol. 5, No. 6, June 1967, pp. 1147–1152.

[3] Peterson, J. P., "Plastic Buckling of Plates and Shells Under Biaxial Loading," TN D-4706, Aug. 1968, NASA.

[4] Ambartsumyan, S. A., "Theory of Anisotropic Shells," TT F-118, May 1964, NASA.

[5] Jones, R. M., "Buckling of Circular Cylindrical Shells with Multiple Orthotropic Layers and Eccentric Stiffeners," *AIAA Journal*, Vol. 6, No. 12, Dec. 1968, pp. 2301–2305.

[6] Block, D. L., Card, M. F., and Mikulas, M. M., Jr., "Buckling of Eccentrically Stiffened Orthotropic Cylinders," TN D-2960, Aug. 1965, NASA.

[7] Budiansky, B., "A Reassessment of Deformation Theories of Plasticity," *Journal of Applied Mechanics*, Vol. 26, June 1959, pp. 259–264.

[8] Stowell, E. Z., "A Unified Theory of Plastic Buckling of Columns and Plates," Rept. 898, 1948, NACA.

[9] Shanley, F. R., "Inelastic Column Theory," *Journal of the Aeronautical Sciences*, Vol. 14, No. 5, May 1947, pp. 261–268.

[10] Nadai, A., *Theory of Flow and Fracture of Solids*, 2nd ed., Vol. I, McGraw-Hill, New York, 1950.

[11] Jones, R. M., "Plastic Buckling of Eccentrically Stiffened Multilayered Circular Cylindrical Shells," TR-0200(S481675)-1, Feb. 1969, The Aerospace Corp., available only from the Clearinghouse CFSTI, Dept. of Commerce.